Chronologically distributed transfection improves AAV2 and AAV2/8 capsid filling and reveals assembly schedule divergence

Qiantong Chen, Chae Hyon Lee, Robert Whitfield, Darren N. Nesbeth

PII: \$2329-0501(25)00205-0

DOI: https://doi.org/10.1016/j.omtm.2025.101610

Reference: OMTM 101610

To appear in: Molecular Therapy - Methods & Clinical Development

Received Date: 17 July 2025

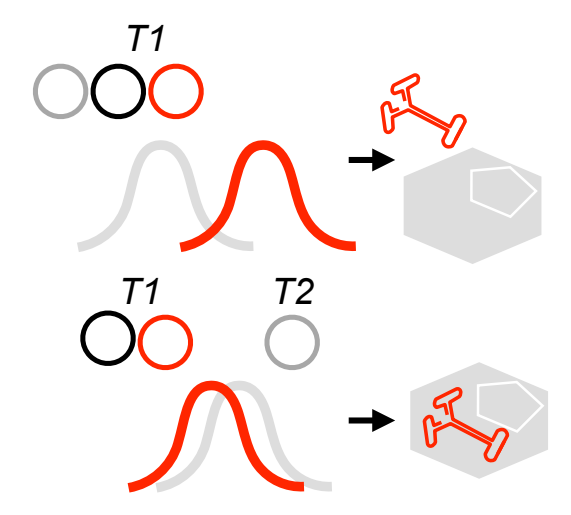
Accepted Date: 1 October 2025

Please cite this article as: Chen Q, Lee CH, Whitfield R, Nesbeth DN, Chronologically distributed transfection improves AAV2 and AAV2/8 capsid filling and reveals assembly schedule divergence, *Molecular Therapy - Methods & Clinical Development* (2025), doi: https://doi.org/10.1016/j.omtm.2025.101610.

This is a PDF file of an article that has undergone enhancements after acceptance, such as the addition of a cover page and metadata, and formatting for readability, but it is not yet the definitive version of record. This version will undergo additional copyediting, typesetting and review before it is published in its final form, but we are providing this version to give early visibility of the article. Please note that, during the production process, errors may be discovered which could affect the content, and all legal disclaimers that apply to the journal pertain.

© 2025 The Author(s). Published by Elsevier Inc. on behalf of The American Society of Gene and Cell Therapy.





Journal President

- 1 Chronologically distributed transfection improves AAV2 and AAV2/8 capsid filling and
- 2 reveals assembly schedule divergence
- 3 Qiantong Chen^{1,2}, Chae Hyon Lee¹, Robert Whitfield², Darren N. Nesbeth^{1*}

4

- ¹Department of Biochemical Engineering, University College London, Bernard Katz Building,
- 6 London WC1E 7JE, UK.
- ²Cytiva Life Sciences, Amersham Place, Little Chalfont, Amersham HP7 9NA, UK.

8

- 9 *Corresponding author: Department of Biochemical Engineering, University College London,
- 10 Bernard Katz Building, London WC1E 6BT, United Kingdom.
- 11 Tel: +44 (0) 20 7679 9582, Fax: +44 (0) 207 916 3943
- 12 Email: d.nesbeth@ucl.ac.uk

Abstract

14

15

16

17

18

19

20

21

22

23

24

25

26

27

28

29

30

31

Adeno-associated virus (AAV) gene therapy vectors often suffer from low capsid filling, resulting in high proportions of empty capsids that reduce efficacy and complicate manufacturing processes. This study investigates whether chronologically distributed transfection could improve capsid filling for AAV2 and AAV2/8 serotypes. We used an empirical approach to test different transfection chronologies by varying the timing of Helper. RepCap, and Payload plasmid delivery across two timepoints, T1 and T2 (24 and 44 hours post-seeding respectively). Our results revealed distinct serotype-specific responses to altered transfection chronologies, with AAV2/8 production being robust to a broader range of chronologies than AAV2. All non-standard chronologies reduced physical and biological titres. Notably, T1 transfection with Helper and Payload plasmids, followed by RepCap plasmid at T2, increased capsid filling efficiency by approximately 7.5-fold for both AAV2 and AAV2/8. This finding provides empirical support for a temporal misalignment hypothesis, whereby suboptimal AAV capsid filling results from capsid assembly occurring before peak genome replication. Our study demonstrates a re-scheduled transfection procedure that can enhance AAV production outcomes and reveals fundamental differences in assembly dynamics between serotypes. These insights contribute to understanding AAV assembly mechanisms and offer a novel method for process development in gene therapy manufacturing.

32

Introduction

35

36

37

38

39

40

41

42

43

44

45

46

47

48

49

50

51

52

53

54

55

56

57

58

59

60

61

62

Recombinant adeno-associated virus (AAV) is a leading gene therapy tool, effecting long-term transgene expression in both dividing and non-dividing therapeutic target cells 1. AAV serotype 2 (AAV2) has strong tropism for neurons and retinal cells, making it particularly suitable for central nervous system and ocular gene therapies ². AAV2/8 exhibits robust liver tropism and ability to cross the blood-vessel barrier, enabling efficient systemic delivery for liver-directed gene therapies ³. AAV production methods typically yield a high proportion of empty capsids lacking the genome encoding the therapeutic transgene, sometimes exceeding 90% of total viral particles 4. Empty capsids can burden manufacturing capacity, complicate downstream purification and reduce efficacy by triggering immune responses and competing with full capsids for cellular receptors 5. Typical AAV production is via transient, three-plasmid (Figure 1.1) co-transfection of HEK293based cells ⁶. The 'Payload' plasmid encodes the therapeutic transgene flanked by inverted terminal repeats (ITRs). The 'RepCap' plasmid encodes AAV Rep and Cap genes, which direct production of four and six proteins respectively 7. ITRs are omitted from the RepCap plasmid to prevent formation of replication-competent AAV virus 8. The 'Helper' plasmid encodes a subset of adenoviral genes that support AAV production but are insufficient for replicationcompetent adenovirus formation, to ensure safety 6, 9. After three-plasmid co-transfection (Figure 1.2), proteins encoded by the Helper and RepCap plasmids bring about targeted replication of the 'payload genome' segment of the Payload plasmid, spanning the two ITRs and the region they flank. These proteins also bring about formation of viral capsid particles and insertion of the payload genome into those particles ^{10, 11}. The precise nature and schedule of the intracellular molecular events that define AAV capsid assembly and genomic filling remains incompletely understood. The potential gene therapy benefits of improving capsid filling with intended genomic payload (the 'empty:full' ratio) motivate ongoing investigation into the events that define AAV particle synthesis and assembly within transiently transfected host cells.

64 The temporal misalignment (TMA) hypothesis

Separation of RepCap genes onto the RepCap plasmid and ITRs onto the Payload may contribute to the lower packaging efficiency observed with recombinant AAV compared to the wild type ¹²⁻¹⁴. Spatial dispersion of RepCap and Payload plasmids within transfected host cells may disrupt the regulatory dynamics of AAV gene expression, impacting the sequence and duration of events that occur in wild-type AAV ¹⁵ and triple transfection ¹⁶. Nguyen et al. developed a general mechanistic model of recombinant AAV assembly which predicted an early peak of capsid synthesis followed by a later peak of payload replication ¹⁷. They interpreted this as a temporal misalignment between capsid assembly and DNA replication, that may contribute to the high 'empty:full' ratio.

This hypothesis was supported by observations reported by Lee at al. ¹⁸, and Lu et al. ^{19, 20}, who engineered separate inducible control into a selection of Helper and RepCap plasmid genes then stably integrated them into HEK293 cells for AAV2 production. Ohba et al. ²¹ engineered inducible control into a version of the Cap gene removed from the context of the RepCap plasmid, and achieved maximal improvement in AAV2 capsid filling by delaying Cap induction

80 dist

until 12 hours after standard three-plasmid transient transfection. Srinivasan et al. ²² distributed the standard three-plasmid transient transfection over two or three separate transfections, with each individual transfection having one half or one third the usual plasmid mass, respectively. Their experimental observations were used to refine a model which again supported a temporal misalignment hypothesis, in which AAV5 capsids formed at an early

stage achieve maximal filling only when accompanied by an optimal expression timing and

Transfection chronologies to test the TMA hypothesis and improve AAV production

abundance of proteins encoded by the Rep gene.

The consistent set of results and simulations from the above reports strongly support temporal misalignment (TMA) as a hypothesis for packaging inefficiency in AAV production from the standard triple-plasmid transient transfection. Specifically, TMA predicts an early peak of

96

101

111

capsid assembly and a later peak of payload replication as a cause of low capsid filling 92 efficiency. Therefore, we sought to apply a new test of the TMA hypothesis by performing a 93 series of novel, chronologically distributed single-, double- and three-plasmid HEK293F cell 94 transfections. We anticipated that empirical screening of seven different transfection 95 chronologies (Table 1) would reveal a pattern of viral filling activities that either aligns with or conflicts with TMA, thereby providing valuable insight into the role of the timing of RepCap, 97 Payload and Helper-encoded gene functions in AAV yield and filling performance. 98 Furthermore, by using only standard plasmids and reagents, we considered that any 99 transfection chronologies that might improve upon the performance of standard methods 100 would be readily implementable by the wider gene therapy bioprocess community, with no requirement for plasmid re-design. 102 We performed chronologically distributed, three-plasmid transfection reactions, with 103 transfection being performed 24 hours ('T1') and 44 hours ('T2') after seeding of host cells and 104 with viral harvest 96 hours after seeding (Figure 1.3). The chronologies we tested included all 105 possible combinations and sequences of 2-plasmid and 1-plasmid transfections. We 106 combined this empirical design with a rational schema, described below, of how the combined 107 actions of the three plasmids lead to AAV particle formation (Figure 1.4) plus three reasonable 108 assumptions regarding AAV production by transient transfection. 109 Our first assumption was that, over time, intracellular plasmid concentration and plasmid gene 110 expression reduce from a post-transfection maximum. Such decreasing plasmid abundance has been observed to result from plasmid degradation ²³, and plasmid dilution by cell division 112 ²⁴. Decreasing expression of plasmid-encoded genes, after a post-transfection maximum, has 113 been reported in the context of mammalian cell transient transfection for production of AAV ²⁵ , lentivirus ²⁶, virus-like particles ²⁷ and recombinant protein ²⁸. 114 115 Our second assumption was that Payload plasmids cannot be packaged in totum into AAV 116 capsids. Payload plasmids are covalently closed circular, double-stranded DNA (dsDNA) 117 molecules, therefore with no exposed 5' phosphate or 3' hydroxyl groups. A typical payload 118 plasmid, such as the pAAV-GFP plasmid used in this study, is 5.7 kilo base pairs in size,

totaling approximately 11,400 nucleotides. This far exceeds the typical AAV packaging capacity of 4.7 kilo bases of single-stranded ²⁹, linear DNA (approximately 4,700 nucleotides). Furthermore, when others have surveyed the range of DNA molecules packaged into a population of AAV virus particles ³⁰⁻³³, no *in totum* Payload plasmids were detected. Our third assumption was that, in the context of multiple (2-3) transfections being performed on the same group of HEK293 cells, prior transfection procedures do not significantly compromise the performance of subsequent transfections in terms of functional transgene expression. This assumption is supported by reports by Cervera et al. ³⁴ and Riedl et al. ³⁵ when using multiple HEK293 transfections to increase the yield of plasmid-encoded recombinant protein.

'Occam schema' as an abductive reasoning aid to predict transfection performance

Results

In recombinant AAV production, the Payload plasmid is the essential initial template substrate for nicking and DNA replication to produce multiple copies of the linear, ITR-flanked, recombinant payload genome (referred to henceforth as 'payload genome(s)' for brevity). It is understood that a combination of host cell functions, and RepCap and Helper plasmid gene functions, all contribute to this process^{7, 30, 36}. In Figure 1.2 we propose an 'Occam schema' of this plasmid-based AAV production, as an abductive reasoning aid to guide our predictions regarding the likely impacts of the seven different transfection chronologies we have trialed. In this schema, we refer collectively to all the combined functions that lead to payload genome production as 'zeta procedures', with the Greek zeta symbol, ζ , as a crude graphical representation of a single-stranded, linear DNA payload genome. Once at least one payload genome has been produced, RepCap and Helper plasmid gene function can then support production and correct filling of capsids, without the absolute requirement for the presence of the Payload plasmid. In Figure 1.2 we refer to these functions that lead to production of correctly packaged capsids as 'theta procedures', with the Greek theta symbol, θ , crudely representing a correctly filled capsid. Our proposed schema

makes no prediction of correctly packaged AAV production dynamics and is not intended as a mechanistic model. However, we use it here as an abductive reasoning aid to guide our predictions regarding the likely impacts of the seven different transfection chronologies we have trialed. Before performing the standard, 'Benchmark', transfection, and seven alternative transfection chronologies, we used the Occam schema of conventional AAV production (Figure 1.2) as a framework for our predictions of the likely impacts of the seven chronologies. We set out these predictions below and provide graphical summaries in Figure 1.4. The uppermost row of Figure 1.4 shows the benchmark (Bmk) transfection chronology, with all three plasmids present in a single transfection performed 24 hours after cell seeding (T1). As all three plasmids are present, ζ - and θ -procedures are both theoretically supported throughout the transfection period. With respect to the TMA hypothesis, we can interpret the Bmk transfection yield performance, in terms of payload genomes, capsids and correctly filled capsids, as being characteristic of the proposed misalignment. Changes to performance against any of these metrics can be interpreted as improvement or exacerbation of the misalignment of assembly events.

Transfection chronologies A, B and C

In Figure 1.4, the row labelled 'A' (Figure 1.4A), depicts the likely impacts of transfection chronology A (Table 1). Only the RepCap plasmid is present in a first transfection performed 24 hours after cell seeding (T1). Helper and Payload plasmids are only provided in a second transfection performed 44 hours after cell seeding (T2). In the context of the Occam schema, no ζ - or θ -procedures are possible for the 44 hours between seeding and T2. During this period, a level of capsid particles may be assembled, albeit at a very low level due to the absence of Helper, but correct capsid filling will be impossible due to the absence of Payload plasmid. For the T2 graphic in Figure 1.4A, we have faded the RepCap plasmid, as we predict that a decrease in RepCap plasmid gene expression during the 72-hour period after T1 is likely to precede the decrease in Payload and Helper plasmid gene expression during the 52-

1/5	nour period after 12 (see Figure 1.3 for timeline). For chronologies B-to-F, the graphics for
176	plasmids used in T2 transfections are faded for the same rationale.
177	Given that ζ - and θ -procedures are impossible for 46% of the post-seeding period for
178	chronology A, as opposed to 25% for the Bmk chronology, we predict an overall reduction in
179	volumetric genome yield performance for transfection A compared to Bmk. Such a result
180	would also be in line with TMA, as, in effect, transfection A exacerbates the misalignment
181	between early capsid production peak and a later payload genome production peak.
182	For transfection chronology B (Table 1, Figure 1.4B) only Payload plasmid is present for T1,
183	Helper and RepCap plasmids only for T2. ζ - and θ -procedures are not possible for the 44
184	hours between seeding and T2, and we predict no payload genome or capsid production
185	during that period as a result. We would expect that, for a fixed amount of RepCap and Helper
186	plasmid, the total amount of Payload plasmid template present would delimit the final yield of
187	payload genomes. As such, compared to the Bmk chronology, for chronology B RepCap and
188	Helper plasmid gene functions are likely to have a lesser amount of Payload plasmid to use
189	as template for ζ -procedures. Overall, we would again predict a reduced genome yield for
190	chronology B, and that this would be consistent with TMA.
191	Transfection chronology C (Table 1, Figure 1.4C) has only Helper plasmid for T1 and as such
192	we suggest the same yield predictions for chronologies A and B would apply, as this plasmid
193	alone is insufficient for payload genome or capsid production. Overall, for transfection
194	chronologies A, B and C, the T1 transfection is a single-plasmid, and therefore insufficient to
195	support ζ - or θ -procedures.
196	
197	Transfection chronology D
198	For transfection chronology D (Figure 1.4D) Payload and RepCap plasmids are present for
199	T1, and Helper plasmid is only provided at T2. We would predict that ζ - and θ -procedures can

take place within the 20-hour T1-T2 intervening period, but to a reduced level of production

compared to Bmk, due to the absence of Helper plasmid for this period. Any rescue of

production from T2 forward, with the addition of Helper plasmid, would be balanced against

200

201

the relatively decreasing contribution of Payload and RepCap plasmid gene function over time. In the context of the TMA hypothesis, chronology D could be predicted to either i) leave net yields unchanged, or ii) further exacerbate misalignment of capsid and payload genome production, depending on which of these processes is more sensitive to the presence of Helper plasmid gene function.

Transfection chronology E

In transfection chronology E (Figure 1.4E) Helper and RepCap plasmids are present for T1, and Payload plasmid is provided at T2. We would predict that neither ζ - or θ -procedures can take place within the T1-T2 intervening period, with only empty capsid production possible. From T2 forward, the addition of Payload plasmid would enable ζ - and θ -procedures to commence, against a background of decreasing relative abundance of Helper and RepCap plasmid gene function over the 52-hour, post-T2 period. Chronology E could be firmly predicted to exacerbate the misalignment of capsid and payload genome production as part of the TMA hypothesis.

Transfection chronology F

For transfection chronology F (Figure 1.4F) Helper and Payload plasmids are present for T1, and RepCap plasmid is provided at T2. Nash et al. 37 and van Lieshout et al. 38 report that Helper plasmid and the intracellular environment are sufficient to support a level of payload genome replication from Payload plasmid template. As such, we would predict that ζ -procedures can take place within the 20-hour T1-T2 intervening period. From T2 the addition of RepCap plasmid enables both ζ - and θ -procedures to commence. Chronology F may remedy the misalignment of capsid and payload genome production of the TMA hypothesis and mimic the wildtype AAV dynamics 17 , by preventing any capsid assembly and Rep synthesis during the first 44 hours of cultivation post-seeding. An increase in an AAV production metric resulting from chronology F may therefore further support the TMA

hypothesis, as well as representing a potential route to improving AAV upstream bioprocessing.

Transfection chronology G

In transfection chronology G (Figure 1.4G) Helper and Payload plasmids are present for T1, and one half the mass of RepCap plasmid used in the Bmk chronology is provided at T1 and T2. In this case, we have depicted the RepCap plasmid graphic as being faded at both these time points to depict this use of half-Bmk mass. We predict that both ζ- and θ-procedures can take place from T1 onward, with the relative abundance of Helper and Payload plasmid gene function declining at a point after T1, while RepCap plasmid abundance has two peaks within the 72-hour period post-T1. We again anticipate that this chronology may remedy capsid and payload genome production misalignment, by distributing the abundance of RepCap over time compared to Bmk chronology (Figure 1.4, uppermost row). As with chronology F, if chronology G increases performance against an AAV production metric, this would be consistent with the TMA hypothesis and may be a promising method for AAV production.

Influence of transfection chronology on production of nuclease-protected viral genomes

To lend this study maximum relevance for the gene therapy bioprocess community, we performed all yield-based experimentation on AAV2 and AAV2/8 serotypes at the lowest scale compatible with statistically rigorous observations. For AAV2 this minimal production scale was 10 mL and for AAV2/8 it was 1 mL. We anticipated that using these scales would lower the barriers to other groups wishing to expand or replicate the results we report. Process development benefits significantly from operating at the smallest practical scale, primarily due to resource efficiency and the ability to explore a broader experimental space. By minimizing the scale, the consumption of costly raw materials such as plasmid DNA, transfection reagents, and cell culture media is substantially reduced, enabling more experimental conditions to be tested within the same budget. This increased throughput is particularly

257	valuable during the initial phases of process development where multiple parameters need to
258	be screened and optimized.
259	We used standard bench-scale procedures for AAV2 and AAV2/8 production by transient
260	transfection and analysis of crude lysate using qPCR (see Materials and Methods, and Tables
261	1-2). This standard qPCR procedure included an incubation with nuclease in order to degrade
262	all DNA present in soluble crude cell lysate material, including unpackaged payload genomes
263	^{39, 40} . We therefore reasoned that all genomes quantified are likely to have been protected by
264	association with capsids capable of sequestering them from nuclease-based degradation.
265	All transfection chronologies achieved or exceeded a minimum level of 108 vg/mL (Figure 2A,
266	2B). These values were three orders of magnitude above the 10 ⁵ vg/mL limit of quantitation
267	(LOQ) for the assay. For both serotypes, chronologies A-E represented a lower plateau of vg
268	yield performance, compared to F and G (Figure 2C, 2D). This is particularly notable when
269	comparing chronologies D and F, where the T1 presence of Helper plasmid (chronology F) is
270	associated with greater vg yield than the T1 presence of RepCap plasmid (chronology D). This
271	is counter to expectations of a greater role for RepCap in payload genome replication and also
272	supports the concept of plasmid presence and cellular protein functions having the ability to
273	'prime' cells for subsequent virus production ^{41, 42} .
274	Payload genome production is possible for 54% of the total post-seeding time period for
275	chronology A, and 75% for chronology D (Figure 1.3). Despite this, the vg/mL yield for AAV2/8
276	chronology A is markedly higher than D (Figure 2D). For AAV2, choronology A and D vg/mL
277	yields are broadly the same (Figure 2C).
278	

279

280

281

282

283

Influence of transfection chronology on production of transducing units

We next used standard bench-scale transduction and flow cytometry procedures to quantify the level of GFP payload genome transfer to HEK293T cells (Figure 3), achieved by the cell lysate material tested in Figure 2. We also determined the fluorescence of untreated target cells and plotted this as a notional TU/mL level to represent the limit of quantitation (LOQ) for

284	the procedure. We interpreted TU/mL levels from transduction experiments that were at or
285	below the LOQ as an abolition of infectiousness.
286	In line with observations reported by Ellis et al ⁴³ , the AAV2, Bmk transfection resulted in crude
287	lysate with a markedly higher TU/mL yield than AAV2/8 (Figure 3). AAV2 chronologies A, B,
288	D and E yielded TU/mL levels at or below LOQ (Figure 3A), while all AAV2/8 chronologies
289	exceeded LOQ (Figure 3B). Comparing the vg/mL data of Figure 2 and the TU/mL data of
290	Figure 3, we concluded that associations between capsids and payload genomes had
291	manifested that were sufficient for nuclease protection but insufficient for infection
292	competence. This may be an indication of the degree to which capsids can adopt a native,
293	infection-competent conformation ^{44, 45} .
294	For AAV2/8, the relative TU/mL yields of chronologies A-G (Figure 3B, 3D) match the pattern
295	of vg/mL yields (Figure 2B, 2D), with chronology D the lowest in both cases. However, for
296	AAV2 this is not the case, with the vg/mL yield pattern for chronologies A-E being inverted for
297	TU/mL with chronology C going from lowest (Figure 2A, 2C) to highest (Figure 3A).
298	Chronology F is the only transfection chronology which, for both AAV2 and AAV2/8,
299	completely omits a plasmid from a transfection timepoint and yields both measurable vg/mL
300	and TU/mL. As such, we selected chronology F, with Bmk as comparator, for analysis by TEM
301	(Figure 4). TEM images revealed that chronology F was able to yield viral particles of
302	comparable gross morphology to the Bmk chronology, for AAV2 and AAV2/8. A
303	comprehensive structural investigation, beyond the scope of this current investigation, will be
304	needed to achieve more conclusive insights. However, we can conclude from these images
305	that, for both AAV2 and AAV2/8, the reduction in TU/mL, from Bmk chronology to chronology
306	F, was not due to total loss of formation of particles with expected gross morphology.
307	
308	We next wished to determine if the yield effects of chronology F were an artefact of unexpected

toxicity or extreme metabolic burden on host cells. To do this we monitored the total number

and viability of transfected cells over the 72 hours post-T1 for chronology F, and the Bmk and

G chronologies as comparators (Figure S1). No major differences between the chronologies

309

310

were observed in terms of viable cell number and viability. This was consistent with observations reported by Cervera et al. ³⁴ and Riedl et al. ⁴⁶, that multiple transfections of a given batch of HEK293 cells did not negatively impact their growth or viability relative to a single transfection procedure.

Influence of transfection chronology on AAV2 capsid yield as determined by ELISA

To determine the level of intact capsid formation for AAV2 transfection chronologies, we used the 'AAV2 Titer Capsid ELISA Kit' (Genscript, Oxford, UK, L00942), which, according to the company recognizes 'intact capsids'. To confirm that the ELISA kit detection was epitope conformation dependent, we used purified AAV2 standards and regular cell lysate samples that had been heated at 75°C for 10 minutes prior to analysis (Figure S2). The heating step resulted in ELISA signal loss, which was consistent with loss of conformational epitope.

Comparing Figure 5A with Figure 3C shows that the relative pattern of AAV2 capsid/mL yield matched the pattern of TU/mL yield, with respect to transfection chronologies. We interpreted this as evidence that, for AAV2, the ability to achieve the conformational epitope recognised

this as evidence that, for AAV2, the ability to achieve the conformational epitope recognised by the ELISA kit antibodies (Figure 5A) correlated with infectiousness (Figure 3C) but did not correlate with ability to protect viral genomes from nuclease activity (Figure 2A, 2C). Furthermore, the formation of capsids capable of protecting genomes from nuclease activity

is less sensitive to transfection chronology than the formation of infectious capsids.

Evidence of AAV2 capsid filling based on ELISA and qPCR data

ELISA and qPCR data can provide a useful indication of the level of correct capsid filling that has been achieved by a given AAV production procedure ⁴⁷. A simple approach is to divide vg/mL by capsids/mL (Figure 5B). For AAV2, this approach was only possible for the chronologies (Bmk, F and G) that yielded measurable capsids/mL levels by ELISA (Figure 5A). For chronologies A to E, although absorbance values were higher than the blank samples (see Materials and Methods), they were still below the ELISA kit's LOQ. Bmk and chronology G both yielded similar levels of capsid filling, with chronology F resulting in an average 7.5-

fold increase in filling. This observation arguably supports our hypothesis that the presence of Helper and Payload plasmid at T1 (Figure 1.3, 1.4) may 'prime' host cells for the subsequent onset of capsid and payload genome production which commences from T2 onward (the latter 54% of the post-seeding period).

344

345

346

347

348

349

350

351

352

353

354

355

356

357

358

359

360

361

362

363

364

365

366

367

340

341

342

343

Inference of AAV2 capsid filling using a novel, ELISA-free method

To further assess the capsid filling level in AAV2, we sought to trial a novel assay for capsid upload that is ELISA-free (A-CUE), which we would then validate by comparison with the more commonly used method based on qPCR and ELISA data. Step 1 of the A-CUE procedure was to normalise cell lysate samples from each AAV2 transfection chronology with respect to vg/mL, to match total vg content and volume. In Step 2 these matched samples were then each incubated with the same amount of Dynabeads™ CaptureSelect™ AAVX Magnetic Beads (referred to from here as 'beads'). These beads have been shown by others to capture AAV2 virus particles in a manner that does not selectively enrich for full or empty capsids 48,49 ^{50, 51}. As such, they are not expected to introduce any bias into concentration procedures and are understood to capture a representative population of AAV2 particles from a given sample. After incubation with lysate, for Step 3 beads were washed and resuspended in the same volume of protein loading buffer for each sample. No elution step was performed. In Step 4 equal volumes of bead solution were analysed by standard acrylamide gel electrophoresis, with the notional vg count in the bead sample being based on the normalised, known vg counts of lysate that had been incubated with beads in Step 1. The gel was processed for Western blotting (Figure 6C) using the Progen B1 antibody, which targets a linear epitope, IGTRYLTR, present in the VP1, VP2 and VP3 capsid monomers of multiple AAV serotypes, including AAV2 and AAV2/8 52. With respect to transfection chronology, the resulting pattern of Western blot antibody binding (Figure 6C) from the A-CUE method approximated the patterns of capsids/mL yield (Figure 5A), as determined by ELISA, and TU/mL yield (Figure 3A, 3C). The similar patterns of A-CUE data, ELISA data and infectivity data for AAV2 (Figures 3, 5 and 6) suggested that the A-CUE

method could be a viable alternative to ELISA for estimating capsid filling in combination with
qPCR data (Figure 6A for workflow). As such, we proceeded to used ImageJ to quantify an
antibody binding signal in each Western blot lane. We termed these quantification values as
'Image Quantification Capsids' (IQ capsids) / lane. We then divided 'IQ capsids' / lane by 'vg
loaded' / lane and plotted this as 'Inferred percentage full capsids' (Figure 6B). These inferred
filling levels arising from the A-CUE procedure closely tracked those determined in Figure 5B
by ELISA and qPCR, with both methods indicating chronologies Bmk and G resulted in similar
filling, while chronology F had an approximately 7.5-fold higher level.

Inference of AAV2/8 capsid filling based on the novel 'A-CUE' procedure

Given the alignment between the ELISA-and-qPCR method and the A-CUE methods for determining AAV2 capsid filling, we next sought to use A-CUE alone to determine AAV2/8 capsid filling, in the absence of an effective AAV8 ELISA kit. We processed samples to the Western blot stage, as before (Figure 6F) and divided the resulting 'IQ capsids' per lane value with the matched 'vg per lane' values to inferr percentage full capsids for each AAV2/8 transfection chronology (Figure 6E). In common with AAV2, the levels of AAV2/8 capsid filling resulting from chronology F were higher than those for the Bmk chronology and chronology G. The Figure 6F Western blot image revealed that every AAV2/8 chronology yielded a detectable level of antibody binding, including a VP3 band which is visible for chronology D upon close inspection. By contrast, AVV2 chronologies B, C and D show now Western blot signal even after close inspection (Figure 6C).

The A-CUE data for AAV2/8 (Figure 6E) suggested that chronologies A, C, D and G all exceeded the capsid filling level of the Bmk transfection. However, this filling pattern for

AAV2/8 did not map onto TU/mL (Figure 3B, 3D) or vg/mL (Figure 2B, 2D) yield performance.

Discussion

With respect to AAV2 process understanding, only transfection chronologies F and G (where both Payload and Helper plasmid were present in the first transfection) yielded both infectious

396	virus and ELISA-positive capsids. All other chronologies abolished either production of
397	infectious capsids or ELISA detection, or both, indicating almost no correctly assembled
398	capsids could be formed in a temporally misaligned AAV2 production process. By contrast, all
399	AAV2/8 transfection chronologies yielded infectious viruses. This difference between AAV2
400	and AAV2/8 is consistent with AAV capsid serotype-specific differences in optimal scheduling
401	of synthesis and assembly events required for correct capsid assembly, observed by Earley
402	et al. ⁵³ .
403	The data in Figure 6 is consistent with transfection chronology F resulting in the highest level
404	of filling for both AAV2 and AAV2/8. Compared to a conventional, benchmark transfection,
405	chronology F has a 20-hour delay in the introduction of RepCap plasmid into host cells that
406	are already theoretically capable of viral genome replication (Figure 1.4). As such, it is possible
407	that chronology F represents a more productive temporal alignment of genome replication,
408	followed by capsid assembly, in agreement with the TMA hypothesis.
409	The AAV2/8 transfection chronology that yielded the lowest TU/mL average overall was
410	chronology D, where both RepCap and Payload plasmids were present at T1 (Figure 3B, 3D).
411	This was lower than chronology A, which featured only RepCap plasmid for the T1
412	transfection. One possibility is that the suboptimal peak of capsid synthesis predicted by TMA
413	was further exacerbated by the presence of both the RepCap and Payload plasmids together
414	(chronology D) compared to the presence of RepCap alone (chronology A).
415	For chronologies B, C and F, RepCap plasmid is only present for 54% of the post seeding
416	period, compared to 75% for the Bmk transfection. As such, capsid yield for B, C and F might
417	be expected to be less than that of Bmk. For AAV2, this is indeed the case, with F having less
418	capsids, and both B and C having no detectable capsids, for both ELISA (Figure 5A) and A-
419	CUE data (Figure 6C). For AAV2/8, while C and E did yield less capsid than Bmk, chronology
420	B yielded significantly more capsid signal then Bmk, as determined by A-CUE procedure
421	(Figure 6F). We interpreted this as evidence of divergence between serotypes in terms of
422	optimal viral assembly schedule. Ohba et al. also reported observations consistent with
423	serotype-based differences in viral assembly schedule. When they placed Cap gene

425

426

427

428

429

430

431

432

433

434

435

436

437

438

439

440

441

442

443

444

445

446

447

448

449

450

451

expression under inducible control for AAV serotypes 1, 2, 3, 5, 6, 7, 8, 9 and 10, only AAV8 did not show an improvement in capsid filling levels when Cap expression was delayed relative to Rep gene expression ²¹. From a bioprocess perspective, for AAV2 and AAV2/8, chronology G matched but did not exceed the performance of the conventional, single transfection benchmark (BmK) procedure in terms of resultant vg/mL, TU/mL and capsid filling. As such, for non-automated systems, the additional human operator labour required for the second transfection would not be justified. Chronology F achieved a 7.5-fold increase in filling for AAV2 (Figures 5 and 6), with a similar increase in filling hinted at in the A-CUE data arising from AAV2/8 (Figure 6). When considering implementation, this process benefit of chronology F would have to be balanced against additional operator labour and the reductions in vg/mL and TU/mL yield performance. For both AAV2 and AAV2/8, there may be a sweet spot between chronologies G and F, where the vg/mL and TU/mL could be enhanced by a small dose of RepCap plasmids delivered alongside Helper and payload at the first point, while the capsid filling levels could be improved by a larger second dose of RepCap at the second time point. Further empirical studies may identify this optimised chronology. In conclusion, our systematic investigation of chronologically distributed transfection revealed several important insights into AAV production dynamics. The most striking finding was the serotype-specific differences in tolerance to varied transfection schedules, with AAV2/8 demonstrating greater robustness than AAV2 across different chronologies, and it suggests bespoke optimization strategies may be needed for each serotype ^{54, 55}. The success of chronology F in improving capsid filling efficiency, particularly for AAV2, provides empirical support for the temporal misalignment hypothesis and suggests that strategic scheduling of plasmid delivery can enhance production outcomes. However, the trade-off between improved filling and reduced overall yields highlights the complexity of optimizing AAV production processes. These findings not only advance our understanding of AAV assembly schedules but also provide practical considerations for process development in gene therapy manufacturing. Future studies combining this chronological approach with

detailed molecular analyses of intracellular events could further elucidate the mechanisms
underlying serotype-specific assembly patterns and guide the development of more efficient
production strategies.

Materials and Methods

Plasmid identities and propagation

AAV genomic payload for all transfections was encoded by pAAV-GFP (Cell Biolabs, AAV-400). AAV2 RepCap genes were encoded by pRC2 (Cell Biolabs,VPK-422). The plasmid pAAV2/8 (Addgene plasmid #112864), encoding AAV2 *Rep* and AAV8 *Cap* genes, was used for AAV2/8 production, and the Helper plasmid for all transfections was pAdDeltaF6 (Addgene plasmid #112867), both kind gifts from James M. Wilson, University of Pennsylvania, USA. Standard molecular biology techniques were used for all plasmid propagation, purification and analytical procedures.

Mammalian cell cultivation

FreeStyle™ HEK293-F cells (Life Technologies Limited, Paisley, UK, catalogue number R79007) were cultivated in FreeStyle™ 293 Expression Medium (Life Technologies, cat. no. 12338018) at 37°C with 5% CO₂ and shaken at 135 rpm inside a humidified incubator (PHC Europe B.V., Loughborough, UK, model MCO-170AICD-PE). Adherent HEK293T cells (Cat .o. CRL-3216) from American type culture collection (ATCC) were cultivated using Dulbecco's modified Eagle's medium (DMEM) with 10% v/v heat inactivated fetal bovine serum (FBS), both purchased from Gibco, UK. Cells were kept at 37°C, 5% CO₂ also in a PHC Europe, model MCO-170AICD-PE, humidified incubator.

Transient transfection

All transfection chronologies are depicted in Table1 and were performed as follows. 24 hours prior to transfection HEK293-F host cells were seeded at 5x10⁵ cells/mL in FreeStyle™ 293

Expression Medium, in either six-well plates (Sarstedt, Germany, 83.3920.500), with a total volume of 1 mL per well, or in 125mL shake flasks (Corning™ 431143) with a total volume of 10 mL per flask. For the benchmark (Bmk) transfection, Helper, RepCap and Payload plasmid solutions were combined at a 1:1:1 molar ratio, to a total mass of 1.5 µg per mL of cell culture and then diluted with Opti-MEM™ (Fisher Scientific, Lough borough, UK, 12559099) to a volume equivalent to 5% of the total cell culture volume. A total of 1.5 μL PElpro® (Sartorius Stedim, Epsom, UK, 101000017) per 1.5 µg of plasmid was diluted with Opti-MEM™ to the same total volume as the plasmid DNA solution. PEI and DNA solutions were then combined and incubated at room temperature for 15 minutes for complex formation. This PEI-DNA solution was then added, dropwise to suspension cell cultures. Transfections with chronologies A-G were performed using the same mass of each plasmid as used in the Bmk transfecion procedure, but split across two transfections, performed at 24 hours and 44 hours after seeding of host cells. Each transfection featured either one or two plasmids, with PElpro® volume scaled down on the basis of a 1:1 PEI volume-to-mass of plasmid ratio (µL:µg). PEI and DNA solutions were each made up to a total Opti-MEM™ volume proportional to the plasmid volume, with specific volumes provided in Table 2. Thes solutions were combine for complexing and added to cells as in the Bmk procedure.

497

498

499

500

501

502

503

504

496

480

481

482

483

484

485

486

487

488

489

490

491

492

493

494

495

AAV harvest

For all transfection procedures, a volume of the Gibco™ AAV-MAX Lysis Buffer (Fisher Scientific, cat. no. 17331899) equivalent to 10% of total cell culture volume was added to host cells 96 hours post-seeding, and the cell culture vessel returned to the incubator for 2 hours under standard cultivation conditions. The total volume of cell culture plus lysis buffer was then transferred to falcon tubes and centrifuged at 4500rpm for 30 minutes at 4°C (Eppendorf, UK, 5910R). The supernatant was gently removed, taking care not to disrupt a small pellet, aliquoted and stored at -80°C prior to further manipulations.

506

507

505

Real-time quantitative PCR (qPCR)

AAV payload viral genomes per mL (vg/mL) in crude lysate were determine by qPCR. A 5 µL crude lysate sample, 35 µL of molecular biology grade water (Corning, UK, 46-000-CM), 5 µL of 10X DNAse I reaction buffer (New England Biolabs, Hitchin, UK, M0303S) and 5 µL of 2 U / µL DNase I (New England Biolabs, Hitchin, UK, M0303S) were added together followed by a 30-minute incubation at 37°C, in order to degrade all DNA not sequestered within AAV capsids. Samples were then incubated at 95°C for 10 mins to denature capsids. Primers of sequence GTCCGCCCTGAGCAAAGA and TCCAGCAGGACCATGTGATC 56 were then added to PCR-amplify the segment of the AAV genome encoding the green fluorescent protein (GFP) open reading frame (ORF). Dilutions of the linearised pAAVGFP plasmid of known purity and concentration, were used to establish a standard curve of cycle threshold (Ct) determinations. Serially diluted samples were mixed with SsoAdvanced Universal SYBR Green Supermix (Bio-Rad, Watford, UK, 1725271) and loaded onto the CFx Connect device (Bio-Rad, UK), set for a 3-minute incubation at 98°C for polymerase activation and DNA denaturation, followed by 39 cycles of amplifications. Each round of amplification consisted of a 15 second, 98°C denaturation step and a 30 s, 60°C annealing/extension step. Melt curve analysis was then performed in an automated manner by the CFx Connect device software.

Enzyme-linked immunosorbent assay (ELISA)

To quantify the number of intact AAV2 particles, the AAV2 Titer Capsid ELISA Kit (Genscript, Oxford, UK, L00942) was used according to the manufacturer's instructions. Briefly, crude lysate samples from AAV2 production and the AAV2 controls provided with the kit were serially diluted and loaded onto a 96-well plate plate coated with the capture antibody. This was followed by incubation with Biotin Anti-AAV2 Antibody and the Streptavidin Horseradish Peroxidase conjugate (Streptavidin-HRP), with washing steps between incubations. The 3,3',5,5'-Tetramethylbenzidine solution (TMB Solution) was then added, followed by Stop Solution. The intensity of the colour in each well was measured at 450 nm and 650 nm using the CLARIOstar® plate reader (BMG LABTECH, Aylesbury, UK). To eliminate the background signal from turbidity, the absorbance at 650 nm was subtracted from the absorbance at 450nm

of the same well. A standard curve was established using a four-parameter logistic (4-PL) model, with the AAV2 control concentration (capsids/mL) plotted on the x-axis and the corresponding mean absorbance value on the y-axis in GraphPad Prism 9.4.1. Limit of quantitation (LOQ) was set up according to the CLSI method guideline EP17-A2 by the manufacturer. It was defined as the actual concentration at which the analyte is reliably detected and at which the uncertainty of the observed test result is less than or equal to the goal set by the laboratory (10% coefficient of variation).

543

544

545

546

547

548

549

550

551

552

553

554

555

556

557

558

559

560

561

562

536

537

538

539

540

541

542

Viral transduction and flow cytometry

50 µL of a solution of adherent HEK293T cells were seeded as target cells at 1 x106 cells/mL in 10% v/v FBS DMEM into each well of a 96-well plate (Fisher Scientific, Loughborough, UK, 10212811) to give a total of 5x10⁴ cells/well. 1 hour post seeding, serially diluted samples of crude lysate were added to each well to 12 µL total volume. 24 hours after lysate sample addition 100 µL of 10% v/v FBS DMEM was added to each well. 72 hours after lysate sample addition all liquid was removed from each well, cells were harvested by standard trypsinisation procedure (Gibco, 25200056) then fixed by incubation with a solution (Thermo Scientific, cat. no. 15424389) of 4% v/v paraformaldehyde solution in phosphate-buffered saline (PBS) for 10 minutes. These fixed cell solutions were centrifuged at 1000 rpm (Eppendorf, 5910R), supernatants removed and cell pellets resuspended in PBS in round bottom 96-well plates (Thermo Scientific, 268200) prior to flow cytometry. To quantify fluorescence arising from viral transfer of the GFP-encoding AAV payload genome, an excitation wavelength of 488 nm was used for the LSRFortessa™ Cell Analyzer Flow Cytometer (BD Biosciences, UK). A minimum of 10,000 cell measurement events were recorded per sample. Data gathered from the flow cytometry experiments were analysed using Flowjo v10.8.1 (BD Biosciences, UK) software. To count the number of live GFP-positive cells, forward and side scatter gating analyses were applied to isolate live cells, forward scatter height and forward scatter area were applied to isolate singlet cells. The percentage of GFP-

positive cells was measured and normalised against non-transduced cells. The number of transducing units /mL was calculated using the following formula:

565

566

563

564

- Equation 1
- 567 TU/mL = {(% GFP positive cells)*(no. cells at transduction)]/vector input volume}*dilution
- 568 factor.

569

570

571

572

573

574

575

576

577

578

579

580

581

582

583

584

585

586

587

588

Bead-capture and electrophoresis of AAV particles

As part of the A-CUE procedure, the vg/mL levels in AAV2 and AAV2/8 cell lysates were used to inform sample dilution with PBS (Fisher Scientific, 12549079) to achieve the same vg concentration and volume (1.8 mL) for all samples for a given serotype (4×108 vg/sample for AAV2, 1 x 108 vg/sample for AAV2/8). These vg-matched samples were then mixed with the same volume of prewashed Dynabead™ CaptureSelect™ AAVX Magnetic Bead solution. The lysate / bead slurry was then placed on a Tube Rotator (Cole-Parmer, TR-200) at 20 rpm for 30 minutes to allow binding to occur. Sample tubes were then placed in an Invitrogen™ DynaMag™-2 Magnet (Fisher Scientific, 10723874) to immobilise the beads. While beads were immobilised, lysate was removed and two PBS washes performed, each with typically 500µL PBS. Washed beads were then resuspended in protein loading buffer which composes of 30 µL 1x Gibco™ AAV-MAX Lysis buffer (Fisher Scientific) plus 9 µL of 4X Laemmli buffer (Bio-Rad, Watford, UK, 1610747) and 1µL of 2-mercaptoethanol (Bio-Rad, Watford, UK, 1610710). This sample was then incubated at 10 min at 95 °C in a ThermoMixer™ C (Eppendorf, UK, 15158953) with the purpose of denaturing capsid proteins such that beadbound particles would disassemble into soluble constituent proteins. Samples were then placed in the Invitrogen™ DynaMag™-2 Magnet (Fisher Scientific, 10723874), supernatant was removed and loaded onto a 10% Mini-PROTEAN® TGX™ Protein Gel for electrophoresis at 160 volts for 40 minutes before being processed for Western blotting.

589

590

Western blotting

PROTEAN® TGX™ Protein Gel were transferred to nitrocellulose membranes using the trans-Blot Turbo Mini 0.2 µm Nitrocellulose Transfer Pack (Bio-Rad, cat. no. 1704158) and the Trans-Blot® Turbo™ Transfer System (model 1704150). Membranes were blocked with EveryBlot Blocking Buffer (Bio-Rad, cat. no. 12010020) for 5 minutes and five five-minute washes with Tris-buffered saline and 0.05% v/v Tween 20 (Bio-Rad, 1706435 and Merck Life Science, Gillingham, UK, P9416) were performed after each antibody incubation step. The anti-AAV VP1/VP2/VP3 mouse monoclonal (PROGEN, cat. no. 690058) was added first, at 1/250 dilution before incubation at room temperature (RT) for 1.5 hour with rocking. Rabbit Anti-Mouse IgG H&L (HRP) antibody (Abcam, Cambridge, UK, AB6728-1001) was then added at 1/2000 dilution prior to 1 hour RT incubation. Bound antibodies were detected using Clarity MAX ECL substrate (Bio-Rad, cat. no. 1705062) and the luminescent image analyzer (Amersham Imager 600, Cytiva). Densitometric analysis of Western blot band intensity was performed using ImageJ (National Institutes of Health, USA) without no manipulation of image brightness or contrast. The acquired images were black/white inverted in ImageJ prior to analysis. The 'Rectangular Selection' tool was used to draw a region of interest (ROI) encompassing each VP protein band and a blank area. The same ROI size was applied to all VP bands to ensure consistency. The intensity of each band in a gel image was normalised by subtracting the intensity of a blank area of the ROI size within the same gel.

610

611

612

613

614

615

616

617

618

591

592

593

594

595

596

597

598

599

600

601

602

603

604

605

606

607

608

609

Transmission Electron Microscopy (TEM)

To prepare samples for TEM, the productions were linearly scaled up to 50 mL for AAV2 and 12.5 mL for AAV8 in 250 mL and 125 mL Erlenmeyer shake flasks (Coring, 431143). After the 72-hour production period, the cell culture was centrifuged at 2000 rpm for 15 min, then resuspended in PBS to 4% of the original cell culture volume. A volume of Gibco™ AAV-MAX Lysis buffer (Fisher Scientific, 17331899) equivalent to 10% of the cell suspension was added, followed by 2-hours incubation under standard cultivation conditions. The cell suspension was subjected to three cycles of freezing and thawing process between a dry ice / 70% ethanol

619	bath and a 37°C water bath. 0.8 µl (200 units) of Benzonase® nuclease (Merck KGaA,
620	Darmstadt, Germany, E1014) was added to each sample and incubated at 37°C for 1 hour.
621	The cell lysate was then centrifuged at 12000 rpm for 10 minutes and the supernatant removed
622	and stored at 4°C prior to purification. Manufacturer's insctructions for the Dynabeads™
623	CaptureSelect™ AAVX Magnetic Beads (Life Technologies Limited, Paisley, UK,
624	2853522001) system were then followed to purify viral particles from crude lysate. Briefly,
625	beads were incubated with sample for 30 minutes before two washes and a final elution step
626	in 60 μL of elution buffer and 6 μL of neutralisation buffer.
627	Formvar/Carbon films on 200 mesh copper grids (TAAB, Berkshire, UK, F077/100) were glow
628	discharged using the PELCO easiGlow machine. 3 µL of purified samples were loaded onto
629	the grid and incubated for 2 min at RT. The excess sample was removed. 3 μL of 1% v/v
630	uranyl acetate was loaded onto the grid and incubated for 40 second at RT. The samples were
631	dried for around 20 minutes prior to imaging with the transmission electron microscope (T12
632	Tecnai Spirit biotwin, FEI).
633	
634	Data availability statement
635	Raw data supporting the findings of this study are available from the corresponding author on
636	request.
637	
638	Author Contributions
639	Conceptualization: QT, RW, DNN, CL. Methodology: QT, CL, RW, DNN. Investigation: QT,
640	CL, RW, DNN. Visualization: QT, CL, RW, DNN. Supervision: QT, CL, RW, DNN. Writing—
641	original draft: QT, RW, DNN. Writing—review & editing: QT, RW, DNN
642	
643	Acknowledgments
644	We gratefully acknowledge the support of the UK Engineering and Physical Sciences

647 **Declaration of interests statement**

- The authors declare that they have no known competing financial interests or personal
- relationships that could have appeared to influence the work reported in this paper.

650

- 651 **Keywords**
- 652 AAV, viral, assembly chronology, transfection, chronofection

653

654 **References**

- 1. Wang, D., Tai, P.W.L. & Gao, G. Adeno-associated virus vector as a platform for gene
- therapy delivery. Nature Reviews Drug Discovery 18, 358-378 (2019).
- 658 2. Planul, A. & Dalkara, D. Vectors and Gene Delivery to the Retina. Annual Review of
- 659 Vision Science 3, 121-140 (2017).
- Wang, L., Wang, H., Bell, P., McMenamin, D. & Wilson, J.M. Hepatic Gene Transfer
- in Neonatal Mice by Adeno-Associated Virus Serotype 8 Vector. Human Gene Therapy 23,
- 662 533-539 (2011).
- 663 4. Wright, J.F. Manufacturing and characterizing AAV-based vectors for use in clinical
- 664 studies. Gene Therapy 15, 840-848 (2008).
- 5. Tse, L.V., Moller-Tank, S. & Asokan, A. Strategies to circumvent humoral immunity to
- adeno-associated viral vectors. Expert opinion on biological therapy 15, 845-855 (2015).
- 667 6. Xiao, X., Li, J. & Samulski, R.J. Production of High-Titer Recombinant Adeno-
- Associated Virus Vectors in the Absence of Helper Adenovirus. Journal of Virology 72, 2224-
- 669 2232 (1998).
- 670 7. Large, E.E., Silveria, M.A., Zane, G.M., Weerakoon, O. & Chapman, M.S. Adeno-
- associated virus (AAV) gene delivery: dissecting molecular interactions upon cell entry.
- 672 Viruses 13, 1336 (2021).

- 673 8. Samulski, R.J., Srivastava, A., Berns, K.I. & Muzyczka, N. Rescue of adeno-
- 674 associated virus from recombinant plasmids: Gene correction within the terminal repeats of
- 675 AAV. Cell 33, 135-143 (1983).
- 676 9. Samulski, R.J., Chang, L.S. & Shenk, T. Helper-free stocks of recombinant adeno-
- associated viruses: normal integration does not require viral gene expression. Journal of
- 678 Virology 63, 3822-3828 (1989).
- 679 10. King, J.A., Dubielzig, R., Grimm, D. & Kleinschmidt, J.A. DNA helicase-mediated
- packaging of adeno-associated virus type 2 genomes into preformed capsids. The EMBO
- 681 Journal 20, 3282-3291-3291 (2001).
- 11. Doshi, J., Couto, E., Staiti, J., Vandenberghe, L.H. & Zabaleta, N. E2A, VA RNA I, and
- 683 L4-22k adenoviral helper genes are sufficient for AAV production in HEK293 cells. Molecular
- Therapy Methods & Clinical Development 32, 101376 (2024).
- 685 12. Ward, P., Clément, N. & Linden, R.M. cis Effects in Adeno-Associated Virus Type 2
- 686 Replication. Journal of Virology 81, 9976-9989 (2007).
- 687 13. Grimm, D., Kern, A., Pawlita, M., Ferrari, F. K., Samulski, R. J. & Kleinschmidt, J. A.
- 688 Titration of AAV-2 particles via a novel capsid ELISA: packaging of genomes can limit
- production of recombinant AAV-2. Gene Therapy 6, 1322-1330 (1999).
- 690 14. Zeltner, N., Kohlbrenner, E., Clément, N., Weber, T. & Linden, R.M. Near-perfect
- 691 infectivity of wild-type AAV as benchmark for infectivity of recombinant AAV vectors. Gene
- 692 Ther 17, 872-879 (2010).
- 693 15. Cao, L., During, M. & Xiao, W. Replication competent helper functions for recombinant
- 694 AAV vector generation. Gene Therapy 9, 1199-1206 (2002).
- 695 16. Liu, H., Liu, N., Zhou, C., Du, A., Kapadia, M., Tai, P.W.L., Barton, E., Gao, G., Wang,
- D. High-purity AAV vector production utilizing recombination-dependent minicircle formation
- and genetic coupling. EMBO Molecular Medicine, 1-20 (2025).
- 698 17. Nguyen, T.N.T., Sha, S., Hong, M.S., Maloney, A.J., Barone, P.W., Neufeld, C.,
- Wolfrum, j., Springs, S.L., Sinskey, A.J. & Braatz, R.D. Mechanistic model for production of

- 700 recombinant adeno-associated virus via triple transfection of HEK293 cells. Molecular
- 701 Therapy Methods & Clinical Development 21, 642-655 (2021).
- 702 18. Lee, Z., Lu, M., Irfanullah, E., Soukup, M. & Hu, W.-S. Construction of an rAAV
- 703 Producer Cell Line through Synthetic Biology. ACS Synthetic Biology 11, 3285-3295 (2022).
- 19. Lu, M., Lee, Z., Lin, Y., Irfanullah, I., Cai, W. & Hu, W. Enhancing the production of
- 705 recombinant adeno-associated virus in synthetic cell lines through systematic
- 706 characterization. Biotechnology and bioengineering 121, 341-354 (2024).
- 707 20. Lu, M., Lin, Y., Kuo, H., Cai, W., Ye, Q., Zhao, L. & Hu, W. Tuning capsid formation
- dynamics in recombinant adeno-associated virus producing synthetic cell lines to enhance full
- 709 particle productivity. Biotechnology Journal 19, 2400051 (2024).
- 710 21. Ohba, K., Sehara, Y., Enoki, T., Mineno, J., Ozawa, K. & Mizukami, H. Adeno-
- 711 associated virus vector system controlling capsid expression improves viral quantity and
- 712 quality. Iscience 26 (2023).
- 713 22. Srinivasan, P., Canova, C.T., Sha, S., Nguyen, T.N.T., Joseph, J., Sangerman, J.,
- Maloney, A.J., Katsikis, G., Ou, R.W. & Hong, M.S. Multidose transient transfection of human
- 715 embryonic kidney 293 cells modulates recombinant adeno-associated virus2/5 Rep protein
- 716 expression and influences the enrichment fraction of filled capsids. Biotechnology and
- 717 Bioengineering 121, 3694-3714 (2024).
- 718 23. Lechardeur, D., Sohn, K. J., Haardt, M., Joshi, P. B., Monck, M., Graham, R. W.,
- 719 Beatty, B., Squire, J., O'Brodovich, H. & Lukacs, G. L. Metabolic instability of plasmid DNA in
- the cytosol: a potential barrier to gene transfer. Gene Therapy 6, 482-497 (1999).
- 721 24. Wang, X., Le, N., Denoth-Lippuner, A., Barral, Y. & Kroschewski, R. Asymmetric
- 722 partitioning of transfected DNA during mammalian cell division. Proceedings of the National
- 723 Academy of Sciences 113, 7177-7182 (2016).
- 724 25. Pistek, M., Andorfer, P., Grabherr, R., Kraus, B. & Hernandez Bort, J.A. Factors
- 725 affecting rAAV titers during triple-plasmid transient transfection in HEK-293 cells.
- 726 Biotechnology Letters 46, 945-959 (2024).

- 727 26. Suleman, S., Fawaz, S., Roberts, T., Ellison, S., Bigger, B. & Themis, M. Optimised
- 728 protocols to generate high titre lentiviral vectors using a novel transfection agent enabling
- 729 extended HEK293T culture following transient transfection and suspension culture. Journal of
- 730 Virological Methods 325, 114884 (2024).
- 731 27. Lecina, M., Puente-Massaguer, E., Strobl, F., Grabherr, R., Striedner, G. & Gòdia, F.
- 732 PEI-mediated transient transfection of high five cells at bioreactor scale for HIV-1 VLP
- 733 production. Nanomaterials. Vol. 10, n. 8 (2020), 1580 (2020).
- 734 28. Li, R. Transient transfection of CHO cells using linear polyethylenimine is a simple and
- 735 effective means of producing rainbow trout recombinant IFN-γ protein. Cytotechnology 67,
- 736 987-993 (2015).
- 737 29. Bennett, A., Mietzsch, M. & Agbandje-McKenna, M. Understanding capsid assembly
- and genome packaging for adeno-associated viruses. Future virology 12, 283-297 (2017).
- 739 30. Taylor, N.K., Guggenbiller, M.J., Mistry, P.P., King, O.D. & Harper, S.Q. A self-
- 740 complementary AAV proviral plasmid that reduces cross-packaging and ITR promoter activity
- in AAV vector preparations. Molecular Therapy Methods & Clinical Development 32 (2024).
- 742 31. Jen, H.-I., Wilkinson, P., Lu, X. & Zhang, W. Residual DNA Impurities in AAV Vectors—
- 743 Nature and Transcription. Molecular Therapy Methods & Clinical Development (2025).
- 744 32. Halbert, C.L., Metzger, M.J., Lam, S.-L. & Miller, A.D. Capsid-expressing DNA in AAV
- vectors and its elimination by use of an oversize capsid gene for vector production. Gene
- 746 therapy 18, 411-417 (2011).
- 747 33. Hauck, B., Murphy, S.L., Smith, P.L., Qu, G., Liu, X., Zelenaia, O., Mingozzi, F.,
- 748 Sommer, J.M., High, K.A. & Wright, J.F. Undetectable transcription of cap in a clinical AAV
- 749 vector: implications for preformed capsid in immune responses. Molecular Therapy 17, 144-
- 750 152 (2009).
- 751 34. Cervera, L., Gutiérrez-Granados, S., Berrow, N.S., Segura, M.M. & Gòdia, F. Extended
- gene expression by medium exchange and repeated transient transfection for recombinant
- protein production enhancement. Biotechnology and bioengineering 112, 934-946 (2015).

- 754 35. Riedl, S.A., Jérôme, V. & Freitag, R. Repeated transient transfection: an alternative for
- 755 the recombinant production of difficult-to-express proteins like BMP2. Processes 10, 1064
- 756 (2022).
- 757 36. Zhang, J., Frabutt, D.A., Chrzanowski, M., Li, N., Miller, L.M., Tian, J., Mulcrone, P.L.,
- Lam, A.K., Draper, B.E., Jarrold, M.F. et al. A novel class of self-complementary AAV vectors
- 759 with multiple advantages based on cceAAV lacking mutant ITR. Molecular Therapy Methods
- 760 & Clinical Development 32 (2024).
- 761 37. Nash, K., Chen, W. & Muzyczka, N. Complete in vitro reconstitution of adeno-
- 762 associated virus DNA replication requires the minichromosome maintenance complex
- 763 proteins. Journal of virology 82, 1458-1464 (2008).
- an Lieshout, L., Ota, S., Adusei, A., Wiberg, E., Costa-Grant, K., Lata, D., Dollive, S.,
- 765 Stanvick, M., Iwuchukwu, I., Golebiowski, D. et al. An Improved Helper Plasmid Containing
- 766 Deletions Within the E4 and E2a Genes Results in Increased Adeno-Associated Virus
- 767 Productivity. Human Gene Therapy 35, 767-776 (2024).
- 768 39. Martinez-Fernandez de la Camara, C., McClements, M.E. & MacLaren, R.E. Accurate
- 769 Quantification of AAV Vector Genomes by Quantitative PCR. Genes (Basel) 12 (2021).
- 770 40. Bucher, K., Rodríguez-Bocanegra, E., Wissinger, B., Strasser, T., Clark, S.J.,
- 771 Birkenfeld, A.L., Siegel-Axel, D., Fischer, M.D. Extra-viral DNA in adeno-associated viral
- 772 vector preparations induces TLR9-dependent innate immune responses in human
- plasmacytoid dendritic cells. Scientific Reports 13, 1890 (2023).
- 774 41. Chung, C.-H., Murphy, C.M., Wingate, V.P., Pavlicek, J.W., Nakashima, R., Wei, W.,
- 775 McCarty, D., Rabinowitz, J., Barton, E. Production of rAAV by plasmid transfection induces
- 776 antiviral and inflammatory responses in suspension HEK293 cells. Molecular Therapy
- 777 Methods & Clinical Development 28, 272-283 (2023).
- 778 42. Mouw, M.B. & Pintel, D.J. Adeno-Associated Virus RNAs Appear in a Temporal Order
- and Their Splicing Is Stimulated during Coinfection with Adenovirus. Journal of Virology 74,
- 780 9878-9888 (2000).

- 781 43. Ellis, B.L., Hirsch, M.L., Barker, J.C., Connelly, J.P., Steininger, R.J., Porteus, M.H., A
- survey of ex vivo/in vitro transduction efficiency of mammalian primary cells and cell lines with
- 783 Nine natural adeno-associated virus (AAV1-9) and one engineered adeno-associated virus
- 784 serotype. Virology Journal 10, 74 (2013).
- 785 44. François, A., Bouzelha, M., Lecomte, E., Broucque, F., Penaud-Budloo, M., Adjali, O.,
- 786 Moullier, P., Blouin, V., Ayuso, E. Accurate Titration of Infectious AAV Particles Requires
- 787 Measurement of Biologically Active Vector Genomes and Suitable Controls. Molecular
- 788 Therapy Methods & Clinical Development 10, 223-236 (2018).
- 789 45. Riyad, J.M. & Weber, T. Intracellular trafficking of adeno-associated virus (AAV)
- vectors: challenges and future directions. Gene Therapy 28, 683-696 (2021).
- 791 46. Riedl, S.A.B., Jérôme, V. & Freitag, R. in Processes, Vol. 10 (2022).
- 792 47. Kontogiannis, T., Braybrook, J., McElroy, C., Foy, C., Whale, A.S., Quaglia, M.,
- 793 Smales, C.M. Characterization of AAV vectors: A review of analytical techniques and critical
- 794 quality attributes. Molecular Therapy Methods & Clinical Development 32, 101309 (2024).
- 795 48. Mietzsch, M., Kamat, M., Basso, K., Chipman, P., Huiskonen, J.T., McKenna, R.
- 796 Structural characterization and epitope mapping of the AAVX affinity purification ligand.
- 797 Molecular Therapy Methods & Clinical Development 32 (2024).
- 798 49. Terova, O., Soltys, S., Hermans, P., De Rooij, J. & Detmers, F. Overcoming
- 799 downstream purification challenges for viral vector manufacturing: enabling advancement of
- gene therapies in the clinic. Cell Gene Ther. Insights 4, 101-111 (2018).
- 801 50. Leibiger, T.M., Remmler, L.A., Green, E.A. & Lee, K.H. Biolayer interferometry for
- 802 adeno-associated virus capsid titer measurement and applications to upstream and
- downstream process development. Molecular Therapy Methods & Clinical Development 32
- 804 (2024).
- 51. Florea, M., Nicolaou, F., Pacouret, S., Zinn, E.M., Sanmiguel, J., Andres-Mateos, E.,
- 806 Unzu, C., Wagers, A.J., Vandenberghe, L.H. High-efficiency purification of divergent AAV
- 807 serotypes using AAVX affinity chromatography. Molecular Therapy Methods & Clinical
- 808 Development 28, 146-159 (2023).

- 809 52. Wobus, C.E., Hügle-Dörr, B., Girod, A., Petersen, G., Hallek, M., Kleinschmidt, J.A.
- 810 Monoclonal antibodies against the adeno-associated virus type 2 (AAV-2) capsid: epitope
- 811 mapping and identification of capsid domains involved in AAV-2-cell interaction and
- neutralization of AAV-2 infection. Journal of virology 74, 9281-9293 (2000).
- 813 53. Earley, L.F., Powers, J.M., Adachi, K., Baumgart, J.T., Meyer, N.L., Xie, Q., Chapman,
- 814 M.S., Nakai, Adeno-associated virus (AAV) assembly-activating protein is not an essential
- requirement for capsid assembly of AAV serotypes 4, 5, and 11. Journal of virology 91,
- 816 10.1128/jvi. 01980-01916 (2017).
- 817 54. Grimm, D. Production methods for gene transfer vectors based on adeno-associated
- 818 virus serotypes. Methods 28, 146-157 (2002).
- 819 55. Khaparde, A., Patra, R., Roy, S., Babu G R, S. & Ghosh, A. Improving AAV Production
- Yield and Quality for Different Serotypes Using Distinct Processing Methods. ACS Omega 10,
- 821 22657-22670 (2025).
- 822 56. Wang, Y., Menon, N., Shen, S., Feschenko, M. & Bergelson, S. A qPCR Method for
- 823 AAV Genome Titer with ddPCR-Level of Accuracy and Precision. Mol Ther Methods Clin Dev
- 824 19, 341-346 (2020).

825

Tables

Table 1. Transfection chronologies used in this study. Overview of transfection chronologies investigated in this study. The benchmark (BmK) procedure introduces all three plasmids (pRepCap, pHelper, and pPayload) in a single transfection at time point T1 (Figure 1.3). Chronologies A-to-F explore various combinations of plasmid delivery timing and grouping across two transfections (T1 and T2). Chronology G is the same as Bmk except that half the RepCap plasmid mass is used in the T1 transfection and the remaining half used in a T2 transfection.

Reaction Code	Transfection 1 (T1) Plasmids(s)			Transfection 2 (T2) Plasmid(s)			
Benchmark (Bmk)	pRepCap	pHelper	pPayload				
Α	pRepCap				pHelper	pPayload	
В			pPayload	pRepCap	pHelper		
С		pHelper		pRepCap		pPayload	
D	pRepCap		pPayload		pHelper		
E	pRepCap	pHelper				pPayload	
F		pHelper	pPayload	pRepCap			
G	(pRepCap)/2	pHelper	pPayload	(pRepCap)/2			

Table 2. Component volumes used in transfections in this study. Component volumes used in DNA transfection reactions across one (T1) or two timepoints (T1 and T2) for serotypes and production volumes indicated. Each reaction condition (Bmk through G) consists of a DNA mixture, containing plasmid DNA diluted in Opti-MEM™ medium, and a polyethylenimin (PEI) mixture, containing PEI diluted in Opti-MEM™ medium. All volumes are recorded in microliters (μL). Volumes indicated are per individual transfection. For all transfections a 'Master Mix' was made with a sufficient volume for a given number of repeats plus one more. As such the smallest volume actually pipetted was 0.66 μL using a Gilson P2 pipette.

		1								
	Transfection		T1				T2			
	chronology	DNA mixture		PEI mixture		DNA mixture		PEI mixture		
		μL Plasmid	μL Opti- MEM™	μL PEI	μL Opti- MEM™	μL Plasmid	μL Opti- MEM™	μL PEI	μL Opti- MEM™	
AAV2 (10 mL)										
1	Bmk	54.8	445.2	15	485	0	0	0	0	
2	Α	4.3	34.6	4.1	131.2	50.5	410.6	10.9	353.8	
3	В	4.4	35.4	2.4	77.8	50.4	409.8	12.6	407.2	
4	С	46.2	375.2	8.5	276	8.6	70	6.5	209	
5	D	8.6	70	6.5	209	46.2	375.2	8.5	276	
6	E	50.4	409.8	12.6	407.2	4.4	35.4	2.4	77.8	
7	F	50.5	410.6	10.9	353.8	4.3	34.6	4.1	131.2	
8	G	52.7	427.9	13	419.4	2.1	17.3	2	65.6	
AA'	V2/8 (1 mL)									
9	Bmk	5.1	44.9	1.5	48.5	0	0	0	0	
10	Α	0.4	3.3	0.4	12.6	4.7	41.6	1.1	35.9	
11	В	0.6	5.4	0.3	9.3	4.5	39.5	1.2	39.2	
12	С	4.1	36.2	0.8	26.6	1	8.7	0.7	21.9	
13	D	1	8.7	0.7	21.9	4.1	36.2	0.8	26.6	
14	E	4.5	39.5	1.2	39.2	0.6	5.4	0.3	9.3	
15	F	4.7	41.6	1.1	35.9	0.4	3.3	0.4	12.6	
16	G	4.9	43.2	1.4	42.2	0.2	1.7	0.2	6.3	

Figures Legends

859

860

861

862

863

864

865

866

867

868

869

870

871

872

873

874

875

876

877

878

858

Figure 1. Illustrative diagrams of AAV genome and caspid production and assembly plasmids and transfection timelines. 1) Simplified diagrams of Payload (red), RepCap (blue), and Helper (green) plasmids. 2) Occam schema of zeta (ζ) procedures, leading to correct payload genome production, and theta (θ) procedures, which require at least one payload genome in order to commence, for production of capsids correctly loaded with payload genomes. 3) Diagram of time points for the transfection chronologies used in this study. At 0 h host cells are seeded, with transfection 1 (T1) 24 h post seeding, T2 44 hours post seeding and harvest 96 h post seeding. The duration of time periods between those four events are also depicted in hours and as a percentage of the 96 h total. 4) Graphical depictions of the eight transfection chronologies used in this study and their predicted consequences. For chronologies A-to-F the following applies: plasmids are depicted as being partially opaque at T2 if they were present at T1. Payload genomes or correctly packaged capsids are absent if their formation is not conventionally understood to be likely or possible. A prediction of empty capsid formation is depicted for the T1 θ procedures whenever payload genome production is predicted to be impossible for the T1 ζ procedures. For chronology G the same rules apply except for the RC plasmid, which is depicted as partially opaque at both T1 and T2, as half the RC plasmid mass of the BmK transfection was used in both transfections. For BmK there is only a single transfection, T1, and no predictions are made for the abundance of any elements at T2, hence no diagrams.

Figure 2. AAV2 and AAV2/8 viral genome yield performance as a function of transfection chronologically. Viral genome titers were determined by qPCR for AAV2 and AAV2/8 crude lysates arising from the transfection chronologies illustrated in Figure 1.4 by letter code, at 10 mL and 1 mL scale respectively. Plots A) and C) show AAV2 results on log and linear scales respectively, while plots B) and D) show AAV2/8 results on log and linear scales respectively. Crude lysate from non-transfected cells (Ntf) were used as qPCR template and interpreted as the limit of quantitation (LOQ) for the assay. The dotted line highlights the lowest yield achieved by any transfection chronology. Error bars represent standard deviation of three biological replicates.

Figure 3. AAV2 and AAV2/8 transducing unit yield performance as a function of transfection chronologically. Volumetric transducing unit titers (TU/mL) were determined by flow cytometry of target cells, to detect GFP expression, for AAV2 and AAV2/8 crude lysates arising from the Figure 1.4 transfection chronologies, at 10 mL and 1 mL scale respectively. Plots A) and C) show AAV2 results on log and linear scales respectively, with the equivalent for plots B) and D) for AAV2/8. Crude lysate from non-transfected cells (Ntf) was incubated wiith target cells and the resulting fluorescence signal interpreted as the LOQ for the assay. The dotted lines and plots A) and B) highlights the lowest yield achieved by any transfection chronology. Error bars represent standard deviation of two-to-four biological replicates.

Figure 4. Transfection chronology F produces particles of standard morphology for AAV2 and AAV2/8. Transmission electron microscopy (TEM) analysis of AAV2 and AAV2/8 viral particles. Representative TEM micrographs showing AAV2 (panels A and D) and AAV2/8 (panels C and F) particles. Benchmark (Bmk) preparations of both serotypes (panels A and C) show characteristic ~28 nm spherical capsids. AAV2 produced using transfection chronology F (panel D, labelled '2F') yielded intact particles similar to benchmark. AAV2/8 produced using transfection chronology F (panel F, labeld '8F') also demonstrated morphology consistent with the benchmark preparation. Panel B (labeled 'X') is the HEK293F cell lysate that had undergone the same production and sample preparation process as Bmk but without the addition of plasmids and panel E (labelled 'Y') is PBS. No particle structures were observed for either. Scale bar in panel 5 is 200 nm and applicable to all panels.

Figure 5. Correctly assembled AAV2 capsid yield and filling as a function of transfection chronology. Panel A) is a plot of ELISA-based quantification of total correctly assembled capsids (capsids/mL) in crude lysates arising from the Figure 1.4 AAV2 transfection chronologies, performed at 10 mL scale. The dotted line highlights the lowest measurable yield achieved. Non-detectable (N.D.) signal resulted from the indicated chronologies. ELISA data were combined with the AAV2 qPCR data plotted in Figure 2 to calculate inferred levels of capsid filling with payload genomes. The full/empty capsid ratios (qPCR/ELISA) were then plotted in panel B), for the chronologies with measurable capsids/mL. Asterisk (*) denotes statistical significance (p < 0.05). Error bars represent standard error of the mean from four biological replicates.

924

925

926

927

928

929

930

931

932

933

934

935

936

937

938

939

940

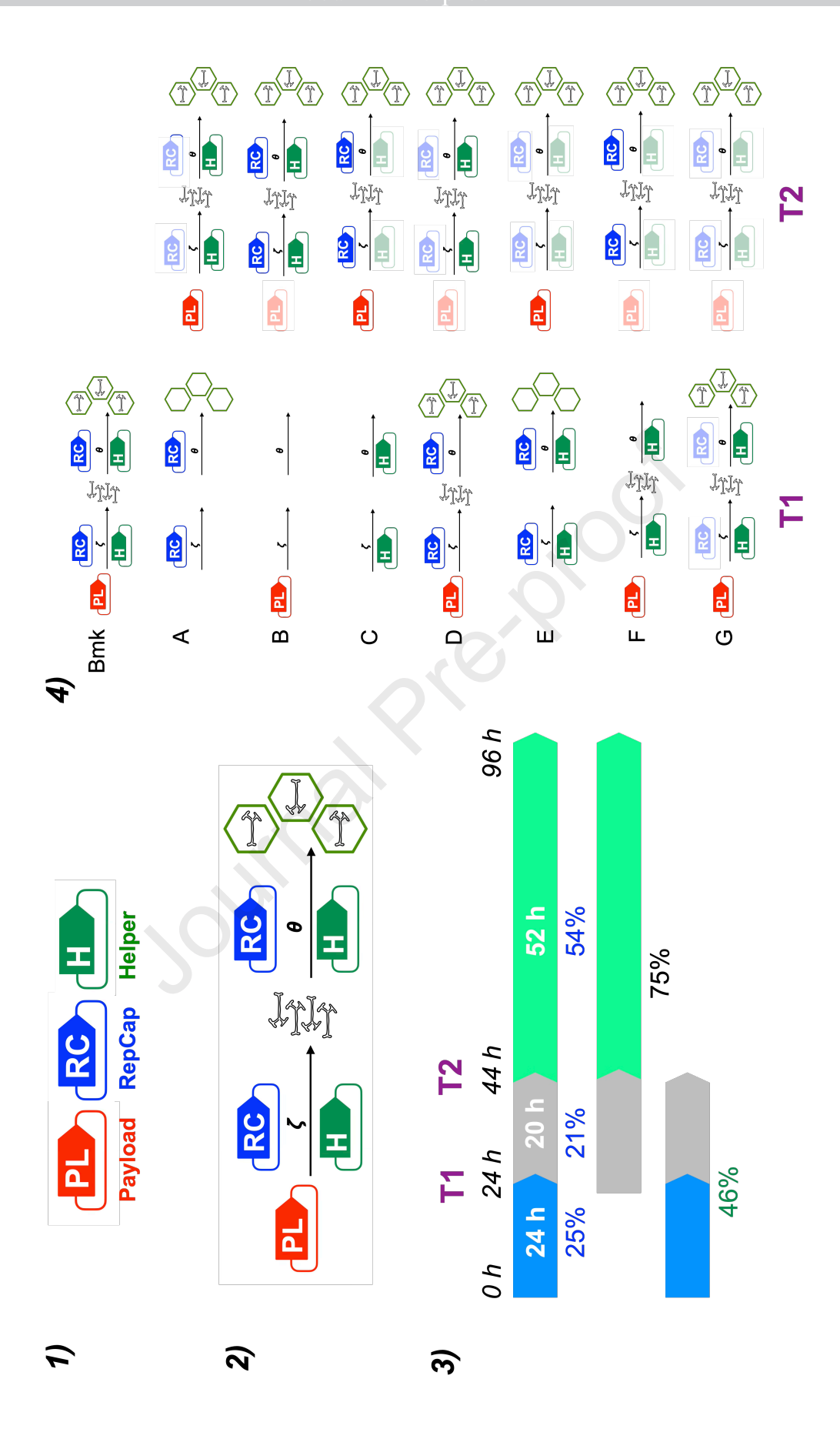
941

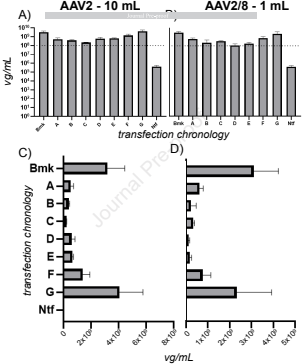
Figure 6. Inferred levels of correct capsid filling using the ELISA-free A-CUE procedure.

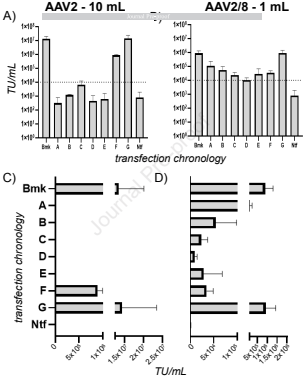
The novel, 'A-CUE', ELISA-free procedure for inferring the level of correct capsid filling with payload genomes is set out in detail in the results section. Panel A) illustrates a workflow whereby the A-CUE method can be validated against ELISA for AAV2. In panel i), comparison of Figure 5A ELISA data and a Western blot image arising from the A-CUE procedure in Figure 6C reveal matching patterns of signal as a function of transfection chronology. As such, when Western blot images (panel C) are quantified by antibody binding signal in a given lane, step ii), they can be combined with Figure 2 qPCR data (step iii)) to calculate an inferred level of correct capsid filling. Panel B) plots this inferred correct filling level as a function of transfection chronology, giving a comparable AAV2 filling pattern to Figure 5B. Panel C) is the Western blot image, annotated by red, purple and black, left-pointing triangles, to indicate the VP1, VP2 and VP3 bands. Thes sizes were inferred by comparison with band migration in the ladder (unlabelled, leftmost lane). Panel D) is the A-CUE data analysis workflow for AAV2/8, which omits step i) due to the lack of ELISA data. Steps ii) and iii) were then followed, based on the panel F) Western blot image and the Figure 2 qPCR data. Resulting inferred level of correct capsid filling were 56plotted in Panel E). Panel F) is the Western blot, annotated as in panel C). For panels C) and F) the gel loading for every transfection chronology was normalised by total number of viral genomes (vg) present in the bead incubation step. For panels B) and E) error bars represent standard deviation from three biological replicates.

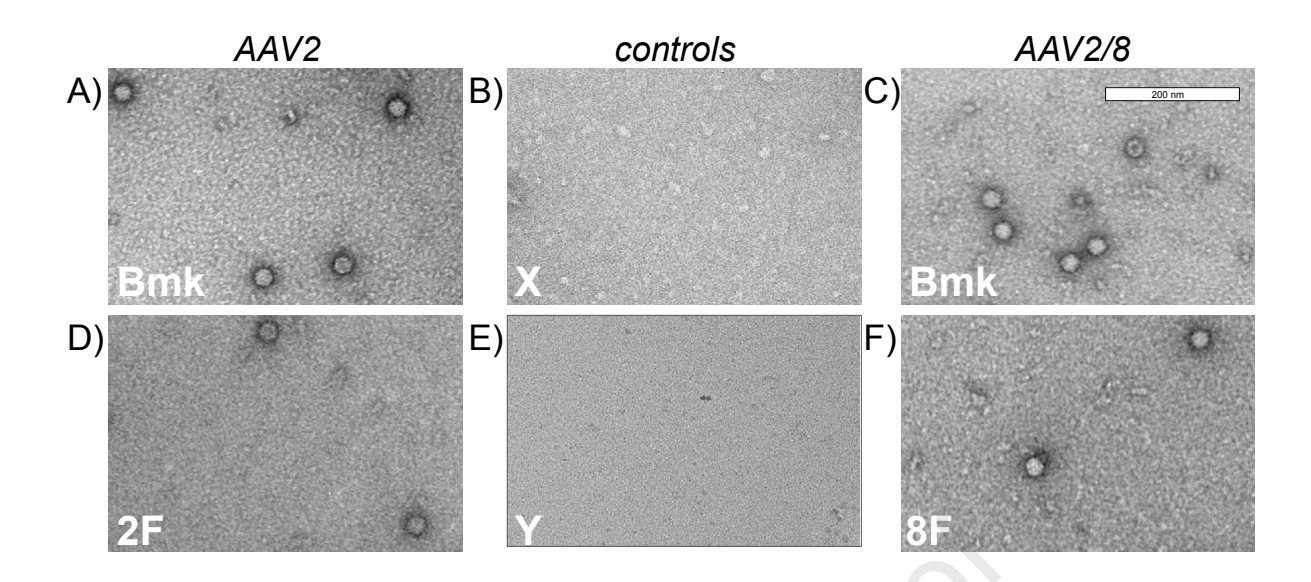
943

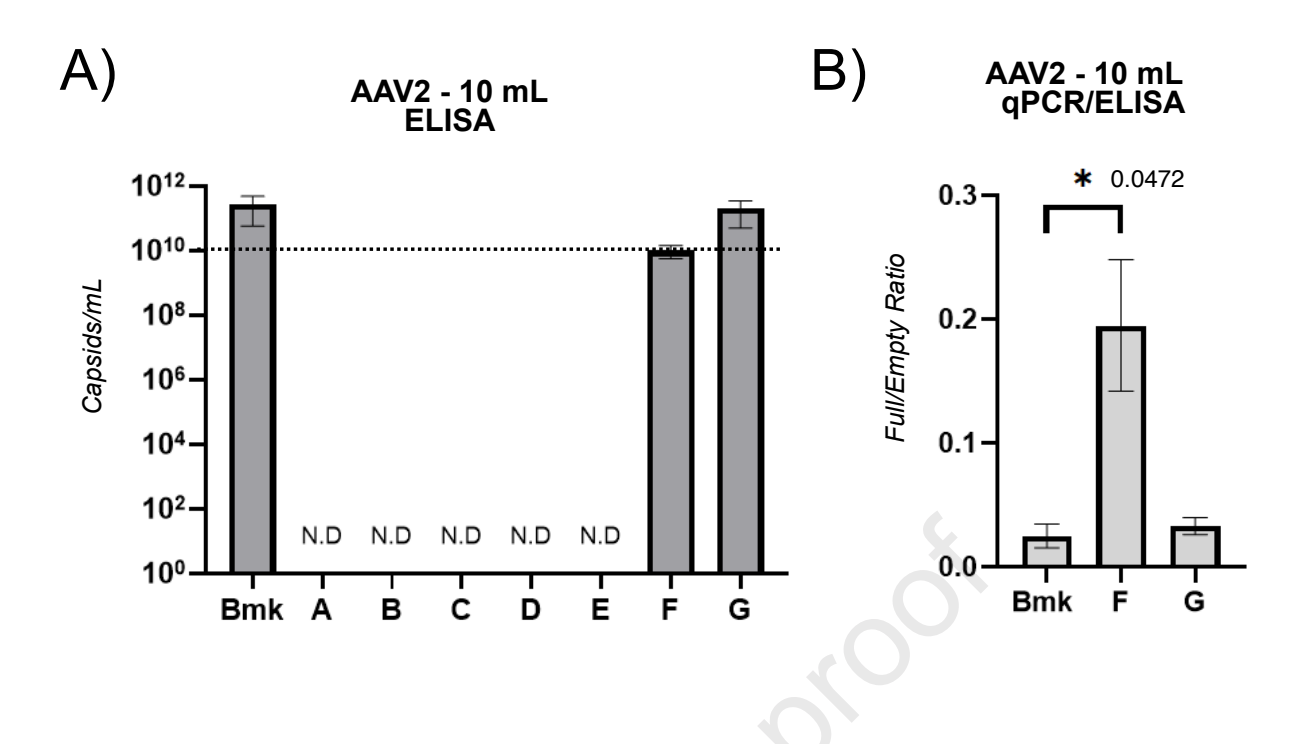
942

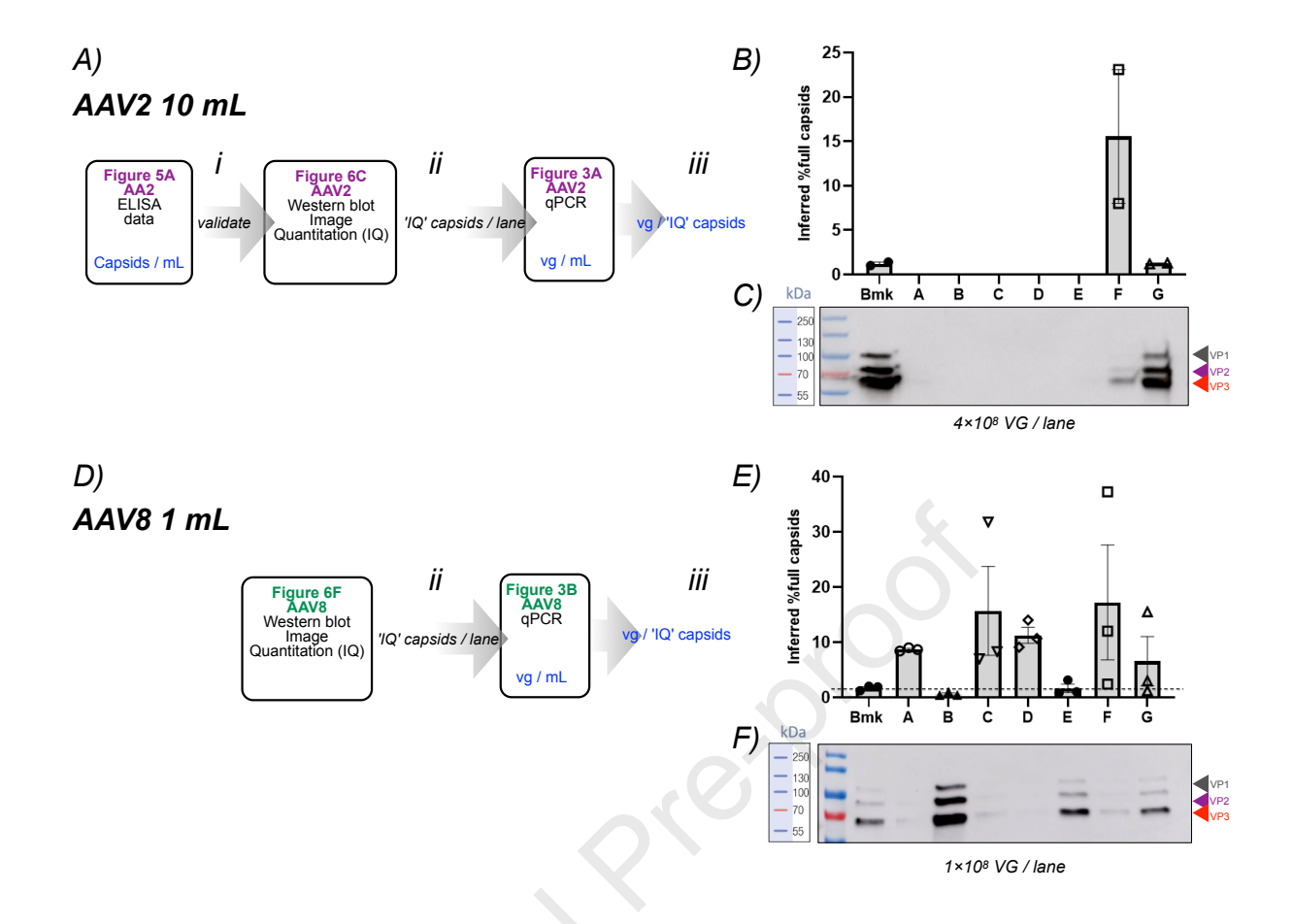












AAV gene therapy vectors suffer from low capsid filling, reducing efficacy. Nesbeth and colleagues tested chronologically distributed transfection timing for AAV2 and AAV2/8 serotypes. Physical and biological titres were always reduced, but delaying RepCap plasmid delivery increased capsid filling 7.5-fold for both serotypes, supporting temporal misalignment hypothesis and offering improved manufacturing methods.